Received: 4 September 2020 | Revised: 5 November 2020 | Accepted: 5 December 2020 | IET Microwaves, Antennas & Propagation

DOI: 10.1049/mia2.12032

The Institution of Engineering and Technology WILEY

ORIGINAL RESEARCH PAPER

Phase shifters with multiple independently controllable bands utilising frequency-selective variable gain networks

Johannes J. P. Venter | **Tinus Stander**

Department of Electrical, Electronic, and Computer Engineering, University of Pretoria, Pretoria, South Africa

Correspondence

Johannes J. P. Venter, Department of Electrical, Electronic, and Computer Engineering, University of Pretoria, Pretoria, South Africa.
Email: Venter.JJP@tuks.co.za

Funding information

South African Radio Astronomy Observatory (SARAO)

Abstract

A dual-band vector-sum phase shifter with independent phase control of the 2.4 and 5 GHz Wi-Fi bands is presented. The network uses band-limited variable gain amplification, with a broadband hybrid coupler at the input and an in-phase recombiner at the output. The circuit is prototyped on RF printed circuit board and exhibits performance characteristics comparable to the state-of-the-art single band vector-sum phase shifters. The prototype achieved an average gain of 2.16 dB over the 2.4 GHz band, with less than 0.26 dB and 1.32° root-mean-square (RMS) gain and phase error across all 2.4 and 5 GHz band tuning states. In the 5 GHz band, an average gain of 0.17 dB is achieved, with less than 0.21 dB and 3.88° RMS gain and phase error. The network's ability to generate band-independent vector modulation over a 12 dB/90° tuning range is demonstrated as well, achieving less than 0.12 dB and 0.27° RMS gain and phase error in the 2.4 GHz band, and less than 0.27 dB and 2.94° gain and phase error in the 5 GHz band.

1 | INTRODUCTION

Phased array antennas and large-scale antenna systems (LSAS) [1] are considered key enabling technologies for future wireless communications. Ideally, LSAS would make use of full digital beamforming, but this is infeasible due to the high cost and power consumption of the mixed-signal components [1,2]. Hybrid beamforming, where analogue and digital beamforming methods are combined, has been shown to be a promising solution in LSAS, enabling spatial multiplexing and multiple-input multiple-output (MIMO) systems [1–4], which increases the link capacity [3]. Shared-aperture antennas could be used as an alternative to increase link capacity, either with multi-band feed ports [5] or separate feed ports for each band [6]. Some work has been done on suitable dual-band and wideband array antennas [7–9], however, current shared-aperture solutions still require separate RF chains in each band (Figure 1a) [10] to enable independent beam-steering of individual bands. This results in an impractically large and costly system when a large number of simultaneous bands are needed.

A potential solution to minimise the number of required RF chains may be the implementation of *channelised beamforming* (Figure 1b) where independent phase shift and gain states may be enforced at different frequencies using a single RF chain. This approach may decrease the number of RF chains required for channelised spatial multiplexing, and enable independent beam-steering for separate bands in a shared-aperture phased array antenna. Before such a solution may be pursued, however, an RF phase shifter or vector modulator with independently tuneable sub-bands is required, of which no suitable examples exist in published literature. The development of such a circuit is the topic of this work.

The RF phase shifters commonly used in hybrid beamforming solutions [11] are designed to feature flat relative phase shifts across the bands of interest [4,11–13]. The phase shifter required in Figure 1b, however, needs to be dispersive in that the relative phase shift ($\varphi_R(\omega)$) is constant over selected frequency bands (f_1 and f_2 in Figure 1b), but a near-arbitrary function of frequency over the full band of operation. This kind of phase shifter may be adapted from several state-of-the-art topologies.

Lumped element all-pass filtering networks implementing second order group delay functions have this property, and have been used as phase shifting networks to implement equi-ripple phase functions across the phase shifter's frequency band of interest [14–16]. Microwave C-sections and generalised coupled-line all-pass phasers have also been demonstrated using distributed elements [17,18]. These all-pass filtering

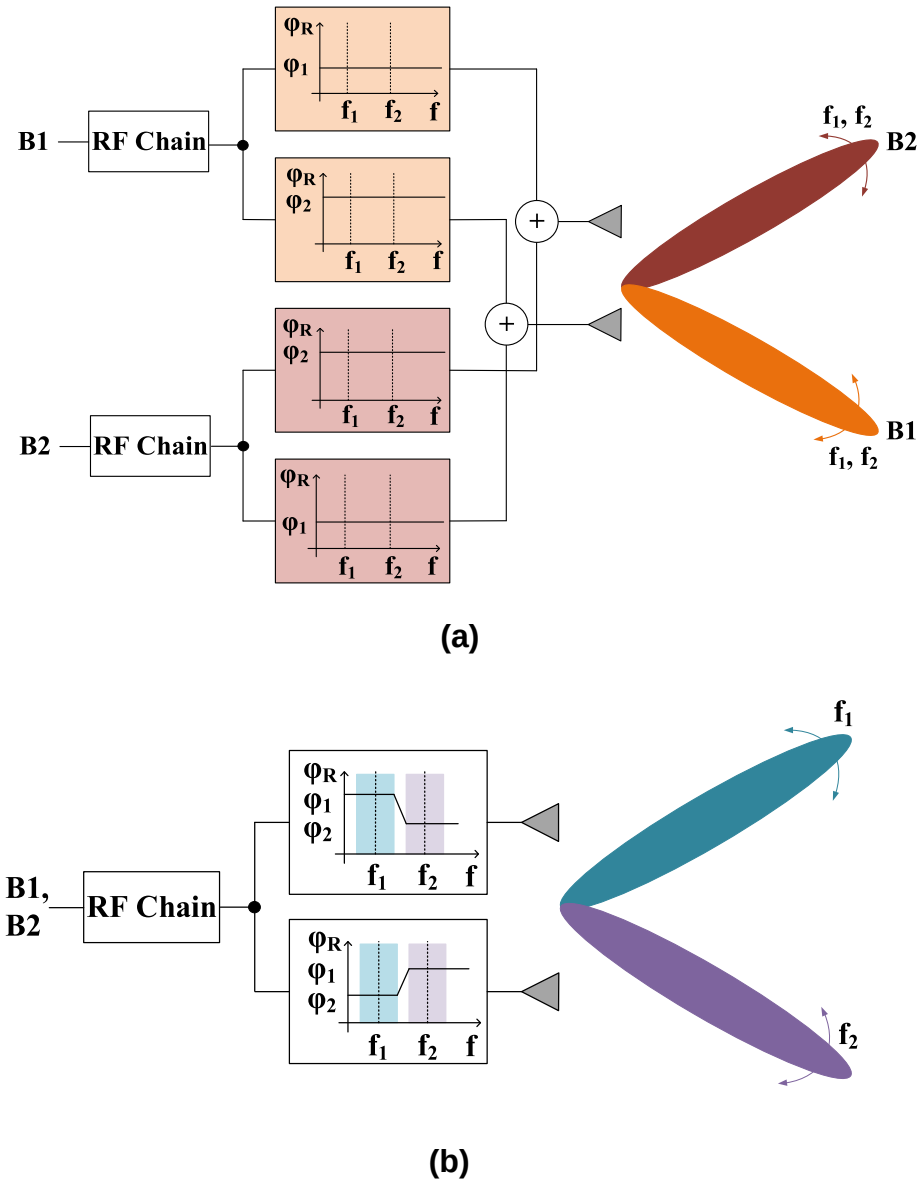

FIGURE 1 Illustration of envisioned phased array frontend using analogue channelised beamforming. (a) Current analogue beamforming architectures. (b) Envisioned analogue channelised beamforming architecture with multi-band independently controllable phase shifting networks

networks themselves have, however, only been demonstrated as fixed networks with no post-production tunability, when used in phase shifter applications. These dispersive phase networks also feature high insertion loss (>3 dB) and passband amplitude error across the frequency bands of interest. Furthermore, none of these networks allow for frequency-limited amplitude control, which negates the possibility of channelised vector modulation. For these all-pass networks to be usable in the design of multi-band phase shifters with independently controllable bands, they would need to be made tuneable; however, post-production tuning of second order all-pass delay networks has also proven problematic [19].

Vector-sum phase shifters (VSPS) are a popular choice in contemporary literature, due largely to their suitability to monolithic microwave integrated circuit (MMIC) integration [20–23]. These may be extended to vector modulators (VM) [12,24], where phase and amplitude control may both be implemented to generate amplitude tapering in the array. VMs may be categorised as active [12,24] or passive [25], depending on whether variable amplifiers or variable attenuators are used. In the implementation of multi-band independently tuneable phase shifters, they are of interest as they replace the problem of creating *frequency-variable phase control* (which often results in large amplitude error, as is evident in most approaches based on second order all-pass delay networks [18]) with the much simpler problem of creating *frequency-variable amplitude control* (which is easily achieved with a range of common RF building blocks, such as filters, diplexers, attenuators and variable-gain amplifiers). In addition, this approach allows for the implementation of amplitude control for vector modulation. Reconfigurable VSPSs have been developed, where the frequency of operation can be dynamically varied by

applying different bias conditions [26,27]. These solutions, however, still do not enable the simultaneous independent tuning of multiple bands on the same RF chain.

Photonic phase shifters have shown promise in achieving extremely large bandwidths at RF frequencies [28,29] and have demonstrated that multi-band VSPS are possible [30]. This is a promising solution to the multi-band phase shifter problem. These photonic devices are not, however, suitable for use in LSAS due to the large size of the auxiliary equipment needed to deploy the solution. In addition, the solution does not lend itself to vector modulation, as amplitude control is not achieved.

This work proposes a vector modulator topology with two independently tuneable bands, implemented using conventional microwave building blocks, utilising frequency-selective variable gain networks to effect the required phase and amplitude responses required for channelised beamforming. This is the first example of a multi-band phase shifter after [30], and the first implemented on RF printed circuit board (PCB) using readily available commercial off-the-shelf (COTS) components.

The article is organised as follows: Section 2 presents the theoretical background of the VSPS, how to extend this theory to the realisation of a multi-band VSPS by utilising frequency-selective variable gain, and the proposed architecture for a multi-band VSPS and VM. In Section 3, the physical implementation of a proof-of-concept dual-band VM is presented. Section 4 presents the measured results of the circuit operating as a VSPS with independent control in the bands, while the circuit's operation as a multi-band VM with independent band control is demonstrated in Section 5. The article is concluded in Section 6.

2 | THEORETICAL BACKGROUND

Conventional VSPS effect relative phase shift by re-combining the amplitude weighted in-phase (I) and quadrature (Q) components of the input signal at the output, as shown in Figure 2. The vector diagram of a conventional VSPS is shown in Figure 3a. The I and Q vectors of the vector-sum phase shifter can be represented as:

$$I = \frac{V_{\text{in}}}{\sqrt{2}} \tag{1}$$

$$Q = j\frac{V_{\text{in}}}{\sqrt{2}}, \tag{2}$$

after passing through the quadrature hybrid. After amplitude weighting of the I and Q signal components, the output signal can be represented by:

$$V_{\text{out}} = \frac{V_{\text{in}}}{\sqrt{2}}\left(A_I + jA_Q\right), \tag{3}$$

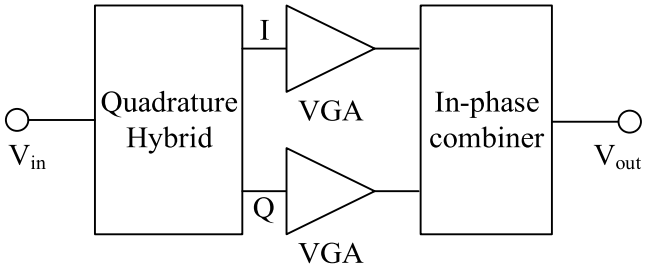

FIGURE 2 Block diagram of vector-sum phase shifter

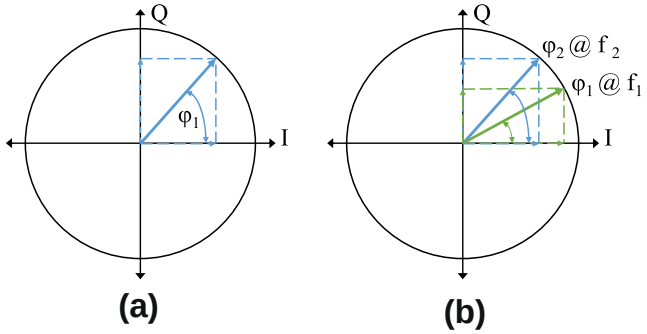

FIGURE 3 Vector diagrams of vector-sum phase shifters: (a) Single band, (b) Dual-band

where, A_I and A_Q are the scalar voltage amplitude weighting factors for the I and Q paths, respectively.

Given this, the output magnitude and relative phase shift ($\Delta\varphi$), in degrees, can be calculated using:

$$|V_{\text{out}}| = \frac{V_{\text{in}}}{\sqrt{2}}\sqrt{{A_I}^2 + {A_Q}^2}, \tag{4}$$

$$\Delta\varphi = \tan^{-1}\left(\frac{A_Q}{A_I}\right) * \left(\frac{180}{\pi}\right). \tag{5}$$

The practically realisable normalised voltage amplitude weighting factors to effect different relative phase shifts (for 40 dB amplitude tuning range) are summarised in Table 1. Full 360° phase rotation would require both positive and negative values of A_I and A_Q, necessitating a selectable phase inversion in each branch not implemented here. In general, A_I and A_Q may be controlled to effect amplitude variation as well (i.e. varying $|V_{\text{out}}|$ in (4)) which results in an IQ vector modulator [12,24], or operated as a vector-sum phase shifter [20–23] which maintains low amplitude error by forcing $|V_{\text{out}}|$ to be constant.

Extending on Equation (5), A_I and A_Q may be given a frequency-selective gain response (still assuming zero relative phase shift in the gain networks over amplitude variation), resulting in:

$$A_I(f_1) = X_I;\ A_I(f_2) = Y_I \tag{6}$$

TABLE 1 Realisable normalised amplitude weighting factors for different relative phase shift states

Δφ (°)	A_I (linear)	A_Q (linear)	A_I (dB)	A_Q (dB)
0	1	0.01	0	−40
10	0.985	0.173	−0.132	−15.221
20	0.937	0.349	−0.563	−9.148
30	0.866	0.500	−1.249	−6.021
40	0.766	0.643	−2.317	−3.836
50	0.643	0.766	−3.836	−2.317
60	0.500	0.866	−6.021	−1.249
70	0.349	0.937	−9.148	−0.563
80	0.173	0.985	−15.221	−0.132
89.4	0.01	1	−40	0

$$A_Q(f_1) = X_Q;\ A_Q(f_2) = Y_Q \tag{7}$$

where, X_I, Y_I, X_Q and Y_Q are all scalar voltage amplitude weighting factors. The frequency-selective responses of A_I and A_Q would lead to V_{out} having different vector angles ($\Delta\varphi$) for f_1 and f_2, effecting a different phase response at different frequencies. The vector diagram of this concept is shown in Figure 3b. This may be extended to N frequency bands, if independent control of $A_{I,Q}$ is established in N bands, resulting in a multi-band VSPS (Figure 4) as opposed to the broadband uniform gain control in Figure 2.

3 | PROOF-OF-CONCEPT IMPLEMENTATION

As proof-of-concept, a dual-band vector-sum phase shifter and vector modulator is implemented (Figure 5) for the 2.4 and 5 GHz Wi-Fi bands ranging from 2.412 to 2.484 GHz and 5.150 to 5.875 GHz. The frequency-selective gain networks are implemented using diplexers to isolate the two bands' amplitude weightings from one another.

The dual-band prototype is implemented in 0.203 mm thick Rogers RO4003 C ($\varepsilon_r = 3.55$), with a 0.85 mm thick FR4 backing for mechanical support and DC routing (Figure 6). The off-the-shelf components used in this design are summarised in Table 2, and include four surface-mount diplexers, one surface-mount broadband quadrature hybrid and one surface-mount in-phase combiner. The MACOM MAAM-0011100 VGAs use a single-ended 50 Ω port interface, and were specifically chosen due to the high gain control range below 10 GHz (larger than 35 dB), which should enable a full 90° relative phase shift range for the VSPS to within 0.6° error (Table 1).

In all cases, simulations were performed using ANSYS HFSS for the full-wave electromagnetic simulations of the layout and Keysight ADS for circuit-EM co-simulations.

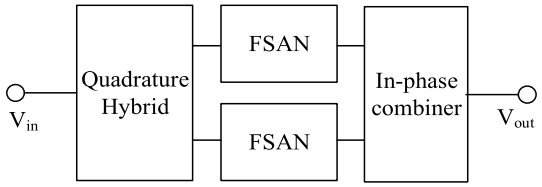

FIGURE 4 Block diagram of multi-band vector-sum phase shifter using frequency-selective amplitude networks (FSAN)

4 | VSPS MEASUREMENT RESULTS

All measurements were carried out on an Anritsu ME4647A VNA, with a two-tier TRL calibration procedure to de-embed the Southwest Microwave SMA end-launch connectors. The prototype's performance is measured according to the control states in Table 3, where the 2.4 GHz band's phase shift is varied from 0° to 90° (in roughly 10° increments) for each 10° increment control step (over the 0°–90° control range) of the 5 GHz band, resulting in a 2D matrix of results for different relative phase shifts. A total of 100 S-parameter measurements were taken, with the root-mean-square (RMS) errors in gain and phase shift calculated over the full band, but also over all control states.

The dual-band phase shifter prototype exhibits less than −17 dB input return loss and −7 dB output return loss across all phase shift states in both frequency bands with (Figures 7 and 8), and average gain (across all phase shift states) of 2.16 and 0.22 dB for the 2.4 and 5 GHz bands, respectively (Figure 9). Table 4 indicates generally good agreement between the expected theoretical, simulated and measured gain values with the error being smaller than 1.3 and 0.2 dB for the 2.4 and 5 GHz bands, respectively.

The prototype has an average DC power consumption of 850 mW due to the high power consumption of the selected VGAs.

A phase shift range of approximately 90° has been achieved for both frequency bands (Figures 10 and 11). Manual tuning was used to control the relative phase shift states, both in simulation and measurement. In a system application, this would also necessitate a calibration procedure as is demonstrated in for example Ref. [31]. Table 5 shows the bias voltages needed for each VGA to affect the required relative phase shifts in the prototype device.

The RMS gain and phase error over a band of interest, when tuning that band's relative phase shift, is calculated as:

$$\Delta A_{\mathrm{RMST2.4,5}} = \sqrt{\frac{1}{NM} \times \sum_{j=1}^{N} \sum_{k=1}^{M} |A_{jk} - A_{avg}|^2} \tag{8}$$

$$\Delta\varphi_{\mathrm{RMST2.4,5}} = \sqrt{\frac{1}{N(M-1)} \times \sum_{j=1}^{N} \sum_{k=2}^{M} |\varphi_{jk} - \varphi_{jk@f_0}|^2} \tag{9}$$

where, N is the number of phase shift states in the band being kept constant (i.e. not being tuned), M is the number of phase shift states in the band being tuned, A_{avg} is the

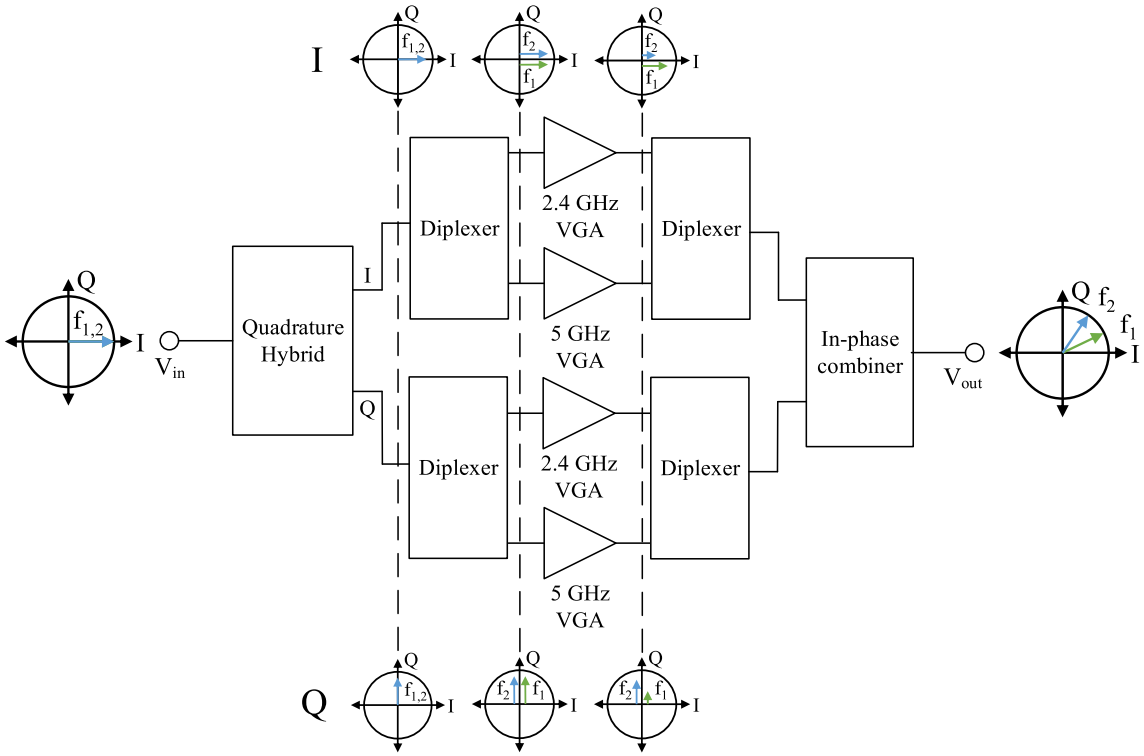

FIGURE 5 Block diagram of dual-band vector-sum phase shifter implementation

average amplitude across all states and $\varphi_{jk@f_0}$ is the relative phase shift at band centre for the specific phase state considered. In the measurements presented here, both j and k would account for 0° to 90° control state measurements in Equation (8), while in Equation (9), j would index control states from 0° to 90° and k would index 10° to 90° (as $k = 1$ is the reference 0° state).

The RMS gain and phase error over a band of interest, when tuning the adjacent band, is calculated as:

$$\Delta A_{\text{RMSC2.4,5}} = \sqrt{\frac{1}{N(M-1)} \times \sum_{j=1}^{N} \sum_{k=2}^{M} |A_{jk} - A_{j1}|^2} \quad (10)$$

$$\Delta \varphi_{\text{RMSC2.4,5}} = \sqrt{\frac{1}{NM} \times \sum_{j=1}^{N} \sum_{k=1}^{M} |\varphi_{jk} - \varphi_{j1}|^2} \quad (11)$$

where, A_{j1} and φ_{j1} are the amplitude and phase of the band being kept constant while the other band is in the reference state. In the measurements presented here, both j and k would account for 0° to 90° control state measurements in Equation (11), while in Equation (10), j would index control states from 0° to 90° and k would index 10° to 90° (as $k = 1$ is the reference 0° state).

The RMS gain and phase errors are shown in Figures 12 and 13. There is excellent correspondence between the simulated and measured results, with less than 0.26 and 0.21 dB RMS gain error and 0.34° and 3.88° RMS phase error when tuning the 2.4 and 5 GHz bands, respectively. Tuning one band leads to less than 0.11 dB RMS gain and 1.32° RMS phase variation in the adjacent band. The constellation diagram for the two bands is shown in Figure 14.

The average measured[1] noise figure (NF) across various phase shift states is shown in Figure 15. A NF of approximately 9.6 and approximately 10.7 dB is obtained for the 2.4 and 5 GHz bands, respectively. The range of NF measurements is shaded in grey (Figure 15), with a ±0.5 dB variance in NF across phase shift states.

A measured[1] input-referred 1 dB compression point (P1dB) of 3 and 5.12 dBm is obtained in the reference state for the 2.4 and 5 GHz bands, respectively (Figure 16). The variance in P1dB for various phase shift states may be attributed to the relationship between P1dB and the attenuation of the VGAs used in the design.

Table 6 compares the proposed dual-band phase shifter performance to the state-of-the-art VSPSs. A figure of merit (FoM) adapted from Ref. [26] to accommodate analogue designs is used for comparison. The FoM is defined as:

$$FoM = \frac{FBW(1)}{Max\{A_{RMS}\}(\text{dB}) * Max\{\Delta\varphi_{RMS}\}(^\circ)}, \quad (12)$$

[1] As no noise or linearity simulation models are provided for the VGAs, only measured data are reported.

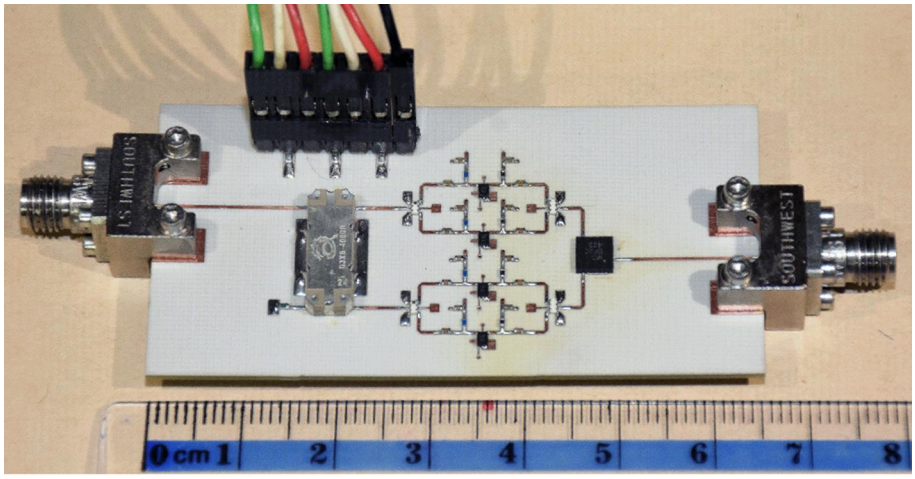

(a)

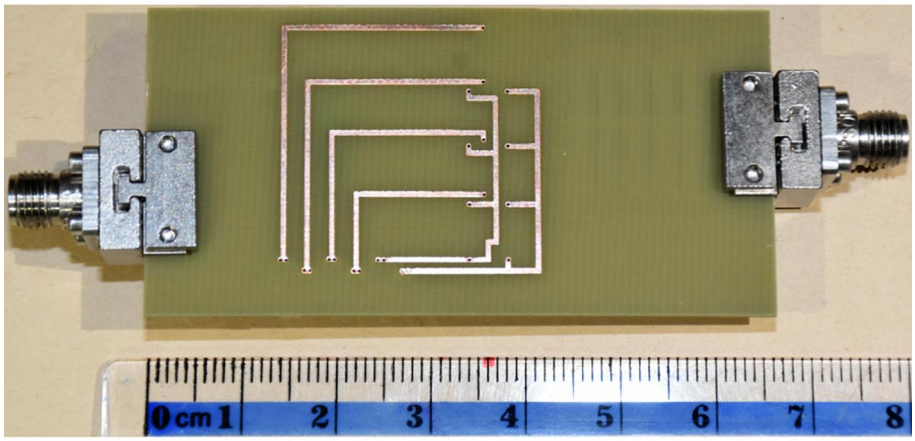

(b)

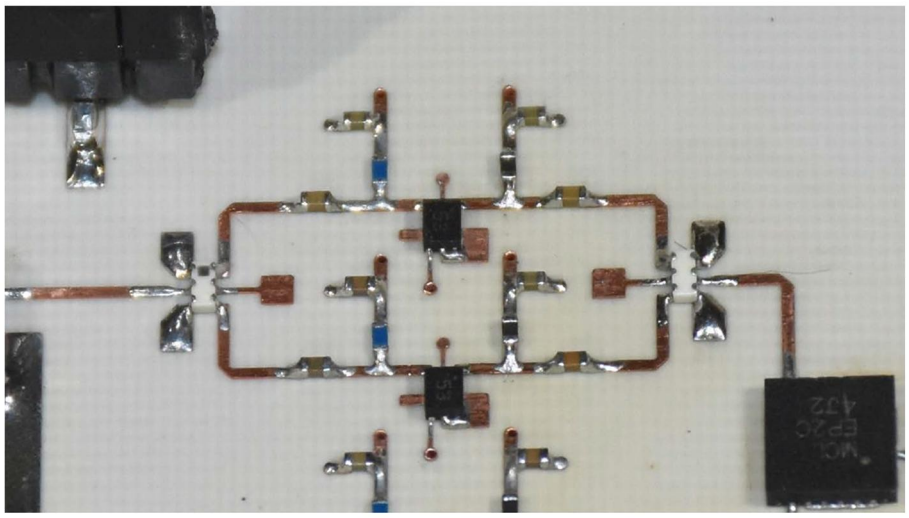

(c)

FIGURE 6 Populated dual-band vector-sum phase shifter. (a) Top view, (b) bottom view and (c) close-up of frequency-selective variable gain network layout

TABLE 2 Summary of COTS components used in dual-band implementation

Function	Component
Quadrature hybrid	Electro-Photonics Hybrid Coupler (Q3XB-4000R)
Diplexer	TDK Multilayer Diplexer (DPX165950DT-8026D1)
VGA	MACOM (MAAM-0011100)
Power combiner	Mini-Circuits Power Splitter/Combiner (EP2C+)

TABLE 3 Control table for different relative phase shift states

	2.4 GHz					
5 GHz	**0**, *0*	**10**, *0*	**20**, *0*	•	**80**, *0*	**90**, *0*
	0, *10*	**10**, *10*	**20**, *10*	•	80, 10	90, 10
	0, *20*	**10**, *20*	**20**, *20*	•	80, 20	90, 20
	•	•	•	•	•	•
	0, *80*	**10**, *80*	**20**, *80*	•	**80**, *80*	**90**, *80*
	0, *90*	**10**, *90*	**20**, *90*	•	**80**, *90*	**90**, *90*

Note: 2.4 and 5 GHz band control states indicated in bold and italic text, respectively.

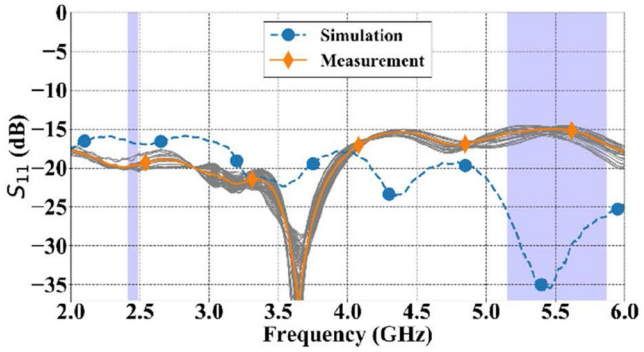

FIGURE 7 Average S_{11}, with measured S_{11}, for all phase shift states, included in grey

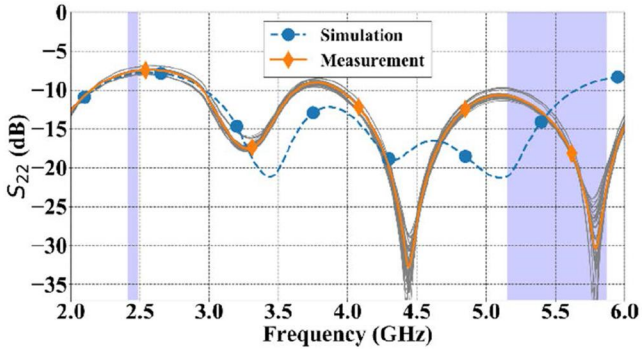

FIGURE 8 Average S_{22}, with measured S_{22}, for all phase shift states, included in grey

where, *FBW* is the fraction bandwidth, $Max\{A_{\mathrm{RMS}}\}$ is the maximum RMS gain error over all 100 measurements (i.e. the worst-case RMS error over the band for all tuning states, as well as all tuning states of the adjacent band), and

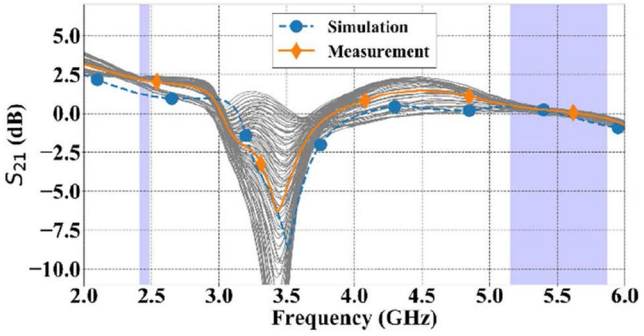

FIGURE 9 Average S_{21}, with measured S_{21}, for all phase shift states, included in grey

TABLE 4 Average gain, across all phase shift states, at band centre frequencies

Band	Analytical calculation	Simulation	Measurement
2.4 GHz	2.50	1.23	2.16
5 GHz	0.19	0.06	0.17

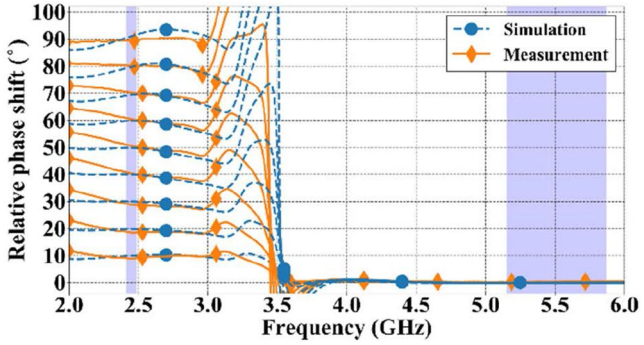

FIGURE 10 Measured relative transmission phase response (S_{21}) when varying the 2.4 GHz band

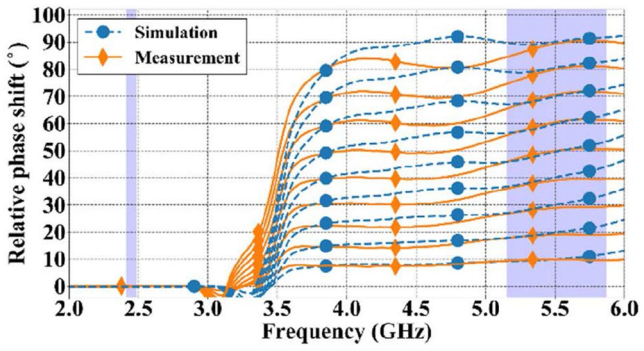

FIGURE 11 Measured relative transmission phase response (S_{21}) when varying the 5 GHz band

$Max\{\Delta\varphi_{RMS}\}$ is calculated, similarly, as the maximum RMS error over all 100 measurements. The proposed dual-band VSPS features a performance is comparable to that which is reported in the current literature, with the added functionality

Measured Δ (°)	2.4 GHz *I* (V)	2.4 GHz *Q* (V)	5 GHz *I* (V)	5 GHz *Q* (V)
0	0.00	−2.00	0.00	−2.00
10	−0.12	−1.14	0.00	−1.14
20	−0.32	−0.94	−0.09	−0.93
30	−0.47	−0.80	−0.42	−0.81
40	−0.59	−0.66	−0.53	−0.71
50	−0.70	−0.54	−0.64	−0.62
60	−0.82	−0.39	−0.73	−0.55
70	−0.97	−0.02	−0.88	−0.47
80	−1.34	0	−1.08	−0.41
90	−1.86	0	−1.56	−0.36

TABLE 5 VGA biasing voltages for different relative phase shift states

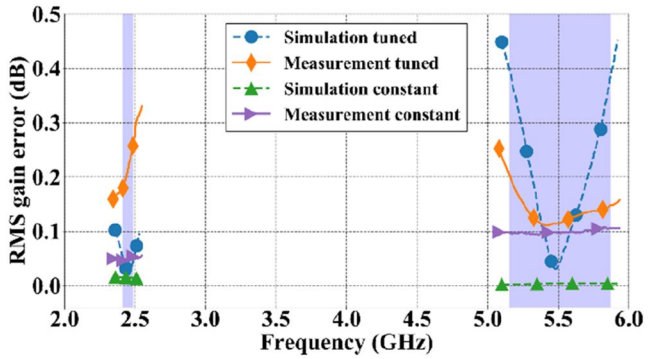

FIGURE 12 RMS gain error. RMS, root-mean-square

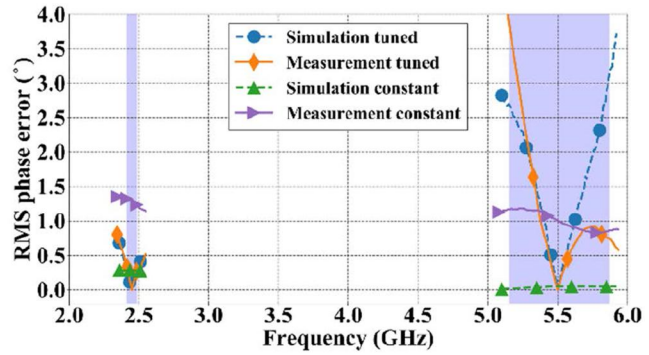

FIGURE 13 RMS phase error. RMS, root-mean-square

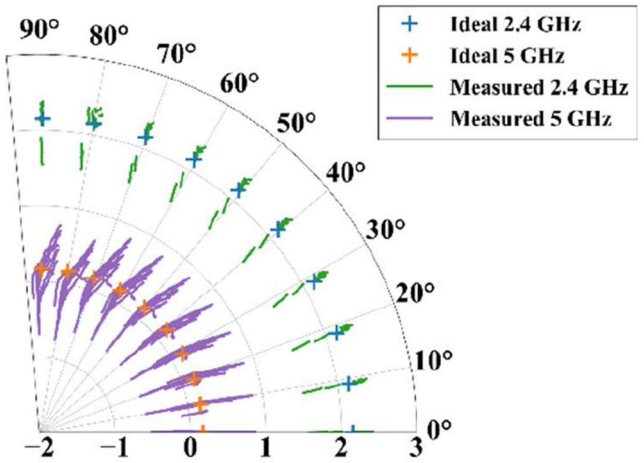

FIGURE 14 Measured constellation diagram in VSPS operation across frequency bands of interest, all 100 measurements included

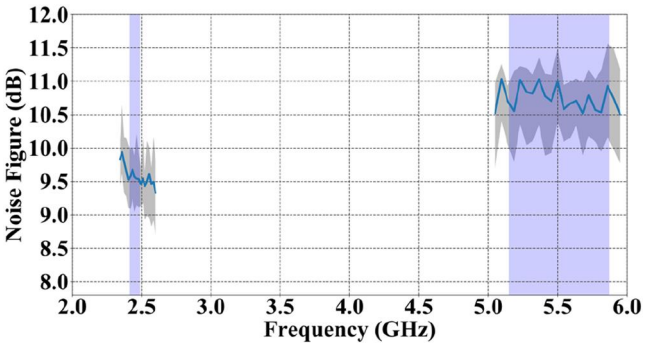

FIGURE 15 Mean NF for relevant frequency bands, with max/min values indicated

of simultaneous and independent relative phase shift control in two separate frequency bands.

5 | VM MEASUREMENT RESULTS

To demonstrate the network's ability to generate band-limited vector modulation, the circuit in Figure 6 was subjected to the relative phase control states in Table 7 for relative attenuation states of 0, 3, 6, 9, and 12 dB, to produce 25 distinct vector modulation states in each of the two bands whilst maintaining the other band in its reference state.

The constellation diagram in Figure 17 indicates maximum RMS gain and phase errors of 0.12 dB, and 0.27° in the 2.4 GHz band, and 0.27 dB and 2.94° in the 5 GHz band over all tuning states. These RMS gain and phase errors were

calculated using Equations (8) and (9), respectively. This compares well with the RMS errors obtained in the state-of-the-art VMs in this frequency range, as shown in Table 8.

6 | CONCLUSIONS

We present a general approach to vector-sum phase shifting and vector modulation with independently controllable bands, implemented using conventional RF blocks. As a proof-of-concept, a dual-band circuit for the 2.4 and 5 GHz Wi-Fi bands is presented. The phase shifter exhibits performance characteristics comparable to the SOTA, with the unique novel property of simultaneous independent control of the two bands' relative phase shifts. The measured prototype has an RMS gain error of 0.26 and 0.21 dB, and an RMS phase error of 0.34° and 3.88° for the 2.4 and 5 GHz bands, respectively. There is minimal interference between the two bands, with less than 0.11 dB RMS gain and 1.32° RMS phase variation when tuning the adjacent band. In addition, the network's ability to generate dual-band independent vector modulation is also presented, with RMS gain and phase errors of 0.12 dB, and 0.27° in the 2.4 GHz band, and 0.27 dB and 2.94° in the 5 GHz band when keeping the other band in the reference state, over 25 vector modulation states.

We have shown that the problem of arbitrary frequency-selective phase control may be substituted with that of arbitrary frequency-selective amplitude control, opening a new avenue for development of a new class of multi-band phase shifter.

The next step in this inquiry will be the application of the proposed circuit in a dual-band array, as shown in Figure 1b. Further future work envisaged beyond this publication includes MMIC implementation, expansion of the phase tuning range to 360° using selectable phase inverters, as well as increasing the number of frequency bands to N (allowing arbitrary phase response profiles) by implementing networks with arbitrary

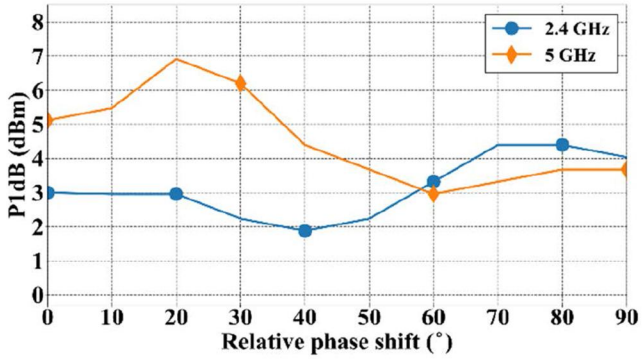

FIGURE 16 P1dB across various phase shifting states

TABLE 6 Comparison of SOTA vector-sum phase shifters

Reference (year)	Frequencies (GHz)	Gain (dB)	RMS gain error (dB)	RMS phase error (°)	Phase tuning range (°)	FoM	Technology	Independent dual-band
Kim & Myung [21] (2000)	2.2–2.3	11.5	0.5	7[b]	310[c]	–	RF PCB	N/A
Lim et al. [32] (2012)	1–2	−3	1.5	2.5	360	0.189	RF PCB	N/A
Mitilineos et al. [33] (2005)	2.4–2.5	2	3[b]	–	90	–	RF PCB	N/A
Qian et al. [23] (2019)	3–7	−1.1	0.89	1.67	360	0.587	40 nm CMOS	No
Yan et al. [27][a] (2013)	2.4–2.5	−15	0.3	4	360	0.034	0.18 μm CMOS	No
Hirai et al. [34] (2019)	2.2–2.6	13	0.2	1.1	360	0.761	0.13 μm SiGe BiCMOS	No
Hirai et al. [35] (2020)	2.2–3.2	13.4	0.15	1	360	2.5	0.13 μm CMOS	No
Zhang et al. [26][a] (2018)	2.4–2.6	6	0.5	2	360	0.080	65 nm CMOS	No
	5.2–5.8		0.62	2.1		0.083		
Bui et al. [30] (2006)	2.4	1.5	3.5[b,c]	–	40	–	Acousto-optic with HiBi fibre	Yes
	5.5	0	3.9[b,c]	–	90	–		
This work	2.41–2.48	2.16	0.26	1.32	90	0.086	RF PCB	Yes
	5.15–5.88	0.17	0.21	3.88	90	0.162		

Abbreviation: PCB, printed circuit board, RMS, root-mean-square.

[a]Frequency reconfigurable.

[b]Not RMS values.

[c]Estimated.

TABLE 7 Vector modulator measured relative phase shift control states for 3 dB relative amplitude attenuation

Control Δ (2.4 GHz/*5 GHz*)	2.4 GHz *I* (V)	2.4 GHz *Q* (V)	5 GHz *I* (V)	5 GHz *Q* (V)
0, *0*	−0.42	−2	−0.46	−2
22.5, *0*	−0.48	−0.77	−0.46	−2
45, *0*	−0.60	−0.55	−0.46	−2
67.5, *0*	−0.79	−0.44	−0.46	−2
90, *0*	−1.85	−0.37	−0.46	−2
0, *22.5*	−0.42	−2	−0.48	−0.97
0, *45*	−0.42	−2	−0.55	−0.71
0, *67.5*	−0.42	−2	−0.73	−0.57
0, *90*	−0.42	−2	−1.76	−0.51

Note: 2.4 and 5 GHz band control states indicated in bold and italic text, respectively. These measurements were repeated for 0, 6, 9 and 12 dB relative attenuation states.

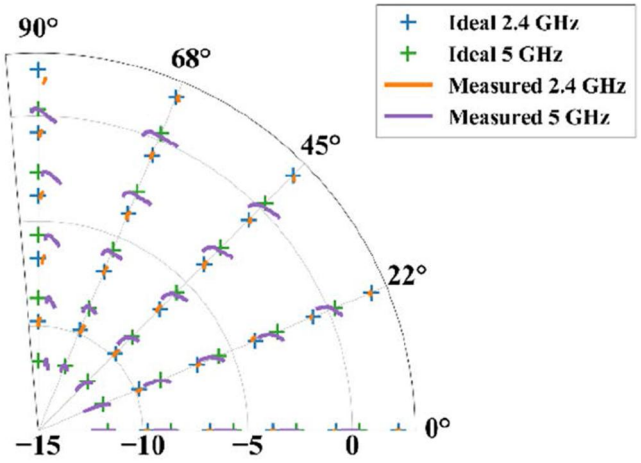

FIGURE 17 Measured constellation in VM operation across frequency bands of interest

TABLE 8 Comparison of RMS errors of SOTA VMs

Reference (year)	Frequency (GHz)	RMS gain error (dB)	RMS phase error (°)
Xia et al. [36] (2019)	0.1–5.7	0.27	1.8
Xu et al. [37] (2017)	0.6–2.8	0.17	2.5
Li et al. [38] (2020)	3.3–22.3	1.5	1.56
Zhang et al. [39][a] (2015)	1.9–2.6	0.2	0.635
Wagner et al. [40] (2015)	1–10	0.16	6
Ivanov et al. [41][a] (2020)	4–6	0.2	1
This work	2.41–2.48	0.15	0.27
	5.15–5.88	0.27	2.94

Abbreviation: RMS, root-mean-square.

[a]Simulated.

transmission magnitude control. The network may also be made bidirectional through implementation of bidirectional VGAs.

ACKNOWLEDGEMENTS

The financial assistance of the South African Radio Astronomy Observatory (SARAO) toward this research is hereby acknowledged (www.sarao.ac.za). The authors wish to thank Electro-Photonics LLC for the hybrid coupler samples used to prototype the design.

ORCID

Johannes J. P. Venter https://orcid.org/0000-0002-8644-8951

REFERENCES

1. Han, S., et al.: Large-scale antenna systems with hybrid analog and digital beamforming for millimeter wave 5G. IEEE Commun. Mag. 53(1), 186–194 (2015)
2. Li, Y.R., et al.: Beam management in millimeter-wave communications for 5G and beyond. IEEE Access. 8, 13282–13293 (2020)
3. Perera, S.M., et al.: Wideband N-beam arrays using low-complexity algorithms and mixed-signal integrated circuits. IEEE J. Sel. Top. Signal Process. 12(2), 368–382 (2018)
4. Ahmed, I., et al.: A survey on hybrid beamforming techniques in 5g: architecture and system model perspectives. IEEE Commun. Surv. Tutor. 20(4), 3060–3097 (2018)
5. Mao, C.-X., et al.: A shared-aperture dual-band dual-polarized filtering-antenna-array with improved frequency response. IEEE Trans. Antenna Propag. 65(4), 1836–1844 (2017)
6. Kong, L., Xu, X.: A compact dual-band dual-polarized microstrip antenna array for MIMO-SAR applications. IEEE Trans. Antenna Propag. 66(5), 2374–2381 (2018)
7. Valavan, S.E., et al.: Planar dual-band wide-scan phased array in X-band. IEEE Trans. Antenna Propag. 62(10), 5370–5375 (2014)
8. Holland, S.S., Schaubert, D.H., Vouvakis, M.N.: A 7–21 GHz dual-polarized planar ultrawideband modular antenna (PUMA) array. IEEE Trans. Antenna Propag. 60(10), 4589–4600 (2012)
9. Tzanidis, I., Sertel, K., Volakis, J.L.: UWB low-profile tightly coupled dipole array with integrated balun and edge terminations. IEEE Trans. Antenna Propag. 61(6), 3017–3025 (2013)
10. Smolders, A.B., et al.: A shared aperture dual-frequency circularly polarized microstrip array antenna. IEEE Antenna Wireless Propag. Lett., 12, 120–123 (2013)
11. Hong, W., et al.: Multibeam antenna technologies for 5G wireless communications. IEEE Trans. Antenna Propag. 65(12), 6231–6249 (2017)

12. Sayginer, M., Rebeiz, G.M.: An eight-element 2-16-GHz programmable phased array receiver with one, two, or four simultaneous beams in SiGe BiCMOS. IEEE Trans. Microw. Theor. Tech. 64(12), 4585–4597 (2016)
13. Kant, G.W., et al.: EMBRACE: a multi-beam 20,000-element radio astronomical phased array antenna demonstrator. IEEE Trans. Antenna. Propag. 56(6), 1990–2003 (2011)
14. Li, H.-Y., Fu, J.-S.: Broadband complementary metal-oxide semiconductor phase shifter with 6-bit resolution based on all-pass networks. IET Microw. Antennas Propag. 9(11), 1144–1151 (2015)
15. Tang, X., Mouthaan, K.: Large bandwidth digital phase shifters with all-pass, high-pass, and low-pass networks. IEEE Trans. Microw. Theor. Tech. 61(6), 2325–2331 (2013)
16. Li, H.-Y., Fu, J.-S.: Analysis of magnetically coupled all-pass network for phase-shifter design. IEEE Trans. Microw. Theor. Tech. 62(9), 2025–2037 (2014)
17. Gupta, S., et al.: All-pass dispersion synthesis using microwave C-sections. Int. J. Circ. Theor. Appl. 42(12), 1228–1245 (2014)
18. Gupta, S., et al.: Generalized coupled-line all-pass phasers. IEEE Trans. Microw. Theor. Tech. 63(3), 1007–1018 (2015)
19. Osuch, P.J., Stander, T.: High-Q second-order all-pass delay network in CMOS. IET Circuits Devices Syst. 13(2), 153–162 (2018)
20. Cetindogan, B., et al.: A 6 bit vector-sum phase shifter with a decoder based control circuit for X-band phased-arrays. IEEE Microw. Wireless Compon. Lett. 26(1), 64–66 (2016)
21. Kim, S.-J., Myung, N.-H.: A new active phase shifter using a vector sum method. IEEE Microw. Guide Wave Lett. 10(6), 233–235 (2000)
22. Mohsenpour, M.-M., Saavedra, C.E.: Variable 360 degree vector-sum phase shifter with coarse and fine vector scaling. IEEE Trans. Microw. Theor. Tech. 64(7), 2113–2120 (2016)
23. Qian, H.J., Zhang, B., Luo, X.: High-resolution wideband phase shifter with current limited vector-sum. IEEE Trans. Circuits Syst. I: Regul. Pap. 66(2), 820–833 (2019)
24. Pepe, D., Zito, D.: Two mm-wave vector modulator active phase shifters with novel IQ generator in 28 nm FDSOI CMOS. IEEE J. Solid State Circ. 52(2), 344–356 (2017)
25. Hameau, F., et al.: A highly linear bidirectional phase shifter based on vector modulator for 60 GHz applications. 2017 IEEE MTT-S International Microwave Symposium (IMS), Honolulu, HI, pp. 1707–1710 (2017)
26. Zhang, Y., et al.: A 1 V 2.4-6 GHz 6-bit vector-sum phase shifter with very low RMS phase error and gain error. Microw. Opt. Technol. Lett. 60(10), 2467–2471 (2018)
27. Yan, T.-C., Lin, W.-Z., Kuo, C.-N.: A 0.75-2.67 GHz 5-bit vector-sum phase shifter. In 2013 European Microwave Integrated Circuit Conference, Nuremberg, pp. 196–199 (2013)
28. Sun, X., et al.: Photonic RF phase shifter based on a vector-sum technique using stimulated brillouin scattering in dispersion shifted fiber. IEEE Trans. Microw. Theor. Tech. 58(11), 3206–3212 (2010)
29. Bui, L.A., et al.: Wide-band RF photonic second order vector sum phase-shifter. IEEE Microw. Wireless Compon. Lett. 15(5), 309–311 (2005)
30. Bui, L., Ghorbani, K., Mitchell, A.: Multi-channel vector sum phase shifter. Opt. Lett. 31(5), 577–579 (2006)
31. Kalyoncu, I., et al.: A phase-calibration method for vector-sum phase shifters using a self-generated LUT. IEEE Trans. Circuits Syst. I: Regul. Pap. 66(4), 1632–1642 (2019)
32. Lim, W., Tang, X., Mouthaan, K.: L-band 360 degree vector-sum phase shifter using COTS components. In 2012 Asia Pacific Microwave Conference Proceedings, Kaohsiung, pp. 100–102 (2012)
33. Mitilineos, S.A., Mitropoulos, G.K., Capsalis, C.N.: A new active RF phase shifter using variable gain, drain voltage controlled PHEMTs: a 2.4-GHz ISM implementation. IEEE Microw. Wireless Compon. Lett., 15(7), 454–456 (2005)
34. Hirai, A., et al.: A vector sum phase shifter with active PPF using transconductance of transistors. In 2019 IEEE Asia-Pacific Microwave Conference (APMC), Singapore, pp. 216–218 (2019)
35. Hirai, A., et al.: Vector-sum phase shifter using a tunable active gm-C polyphase filter. IEEE Trans. Microw. Theor. Tech. 68(10), 4091–4102 (2020)
36. Xia, J., et al.: A 0.1-5.7 GHz CMOS phase shifter with 0.27dB/1.8° RMS magnitude/phase errors and enhanced linearity. In 2019 IEEE 19th Topical Meeting on Silicon Monolithic Integrated Circuits in RF Systems (SiRF), Orlando, FL, USA, pp. 1–3 (2019)
37. Xu, Y., Xia, J., Boumaiza, S.: A 0.6–2.8GHz CMOS RF vector multiplier with low RMS magnitude and phase errors and high P1dB. In 2017 IEEE MTT-S International Microwave Symposium (IMS), Honolulu, HI, pp. 2015–2017 (2017)
38. Li, T., Park, J.S., Wang, H.: A 2–24GHz 360° full-span differential vector modulator phase rotator with transformer-based poly-phase quadrature network. IEEE Trans. Very Large Scale Integr. Syst. (2020), to be published.
39. Zhang, P., et al.: A 6-bit phase shifter with low RMS phase error and flat gain across 1.9–2.6GHz. In 2015 Asia-Pacific Microwave Conference (APMC), Nanjing, pp. 1–3 (2015)
40. Wagner, J., et al.: Broadband inductorless vector modulator IC for localisation and communication systems. Electron. Lett., 51(10), 767–769 (2015)
41. Ivanov, M.A., Podyacheva, A.A., Rumyancev, I.A.: Vector modulator for 5G transceivers in 65 nm CMOS. In 2020 IEEE Conference of Russian Young Researchers in Electrical and Electronic Engineering (EIConRus), St. Petersburg and Moscow, pp. 130–133 (2020)

How to cite this article: Venter JJP, Stander T. Phase shifters with multiple independently controllable bands utilising frequency-selective variable gain networks. *IET Microw. Antennas Propag.* 2021;15:143–153. https://doi.org/10.1049/mia2.12032